International Journal of Minerals, Metallurgy and Materials
Volume 22, Number 9, September 2015, Page 917
DOI: 10.1007/s12613-015-1150-7

Sintering behaviors and consolidation mechanism of high-chromium vanadium and titanium magnetite fines

Mi Zhou, Tao Jiang, Song-tao Yang, and Xiang-xin Xue

School of Materials and Metallurgy, Northeastern University, Shenyang 110819, China
(Received: 10 July 2014; revised: 20 September 2014: accepted: 22 September 2014)

Abstract: To achieve high efficiency utilization of high-chromium vanadium–titanium magnetite (V–Ti–Cr) fines, an investigation of V–Ti–Cr fines was conducted using a sinter pot. The chemical composition, particle parameters, and granulation of V–Ti–Cr mixtures were analyzed, and the effects of sintering parameters on the sintering behaviors were investigated. The results indicated that the optimum quicklime dosage, mixture moisture, wetting time, and granulation time for V–Ti–Cr fines are 5wt%, 7.5wt%, 10 min, and 5–8 min, respectively. Meanwhile, the vertical sintering speed, yield, tumbler strength, and productivity gains were shown to be 21.28 mm/min, 60.50wt%, 58.26wt%, and 1.36 $t \cdot m^{-2} \cdot h^{-1}$, respectively. Furthermore, the consolidation mechanism of V–Ti–Cr fines was clarified, revealing that the consolidation of a V–Ti–Cr sinter requires an approximately 14vol% calcium ferrite liquid-state, an approximately 15vol% silicate liquid-state, a solid-state reaction, and the recrystallization of magnetite. Compared to an ordinary sinter, calcium ferrite content in a V–Ti–Cr sinter is lower, while the perovskite content is higher, possibly resulting in unsatisfactory sinter outcomes.

Keywords: magnetite; chromium; vanadium; titanium; ore sintering; consolidation; mineralogy

1. Introduction

Vanadium–titanium magnetite ore is a complex iron ore that contains various valuable metal elements including iron, vanadium, and titanium. Vanadium–titanium magnetite ore is a major source of vanadium and is most commonly found in Australia, China, Russia, and South Africa [1]. Many studies on the comprehensive utilization of this material have been conducted worldwide [2–6]; however, due to the many drawbacks involved in its use, vanadium–titanium magnetite has been classified as a typical polymetallic paragenetic ore that is difficult to treat and utilize [7–8]. The disadvantages associated with vanadium–titanium magnetite include poor grade, fine mineral crystal size, complicated phase structure, and numerous mineral components [9]. Many researchers have attempted to employ a direct reduction process to realize the effective comprehensive utilization of vanadium–titanium magnetite [10–11]; however, the mainstream route for its comprehensive utilization is the transition from a blast furnace to a basic oxygen furnace (BF→BOF). As the primary charging form for BF, sintering plays an important role in the BF process. In addition, V–Ti–Cr sinter is an important product in achieving the utilization of V–Ti–Cr fines.

To date, the sintering behaviors and consolidation mechanisms of V–Ti–Cr fines have not yet been made clear, significantly influencing the productivity, sinter quality, coke content, sinter cost, BF performance, and furnace life of these materials.

In this study, the chemical composition, particle parameters, and granulation of V–Ti–Cr mixtures were investigated. The effects of quicklime dosage, mixture moisture, wetting time, and granulation time on the behaviors, and metallurgical properties including sinter rate, yield, tumbler strength (TI), and productivity were also studied. Additionally, the consolidation mechanism of V–Ti–Cr fines was clarified using optical microscopy equipped with a Leica Qwin image processing and analysis application, scanning electron microscopy (SEM), and energy dispersive X-ray spectroscopy (EDS).

Corresponding author: Xiang-xin Xue E-mail: xuexx@mail.neu.edu.cn

2. Experimental

2.1. Experimental materials

The V–Ti–Cr fines used in this study were imported from ARICOM Group Company, Russia, and the other raw materials were supplied by Jianlong Iron and Steel Group Company, China. The chemical compositions of the raw materials and coke breeze used in experiments are listed in Tables 1 and 2. Compared with vanadium and titanium magnetite in Panzhihua, China (TFe ~51.16wt%, V_2O_5 ~0.55wt%, TiO_2 ~13.29wt%, Cr_2O_3 <0.08wt%) [12], V–Ti–Cr fines are a high-chromium (Cr_2O_3 0.47wt%), high-vanadium (V_2O_5 1.01wt%), and low-titanium (TiO_2 5.12wt%) vanadium–titanium magnetite ore with a higher utilization value.

The particle parameters of the V–Ti–Cr fines were tested by a dynamic image particle analyzer (BT-1600; Table 3), and the morphological appearance of the V–Ti–Cr fines is shown in Fig. 1. As shown in Table 3, the circularity and aspect ratio of V–Ti–Cr fines are 0.87 and 1.38, respectively, and the fines are difficult to granulate due to the nearly circular particle shapes (Fig.1).

Table 1. Chemical composition of raw materials wt%

Raw materials	TFe	FeO	CaO	SiO_2	MgO	Al_2O_3	TiO_2	V_2O_5	Cr_2O_3	H_2O
V–Ti–Cr fines	61.42	28.63	0.32	2.54	1.20	2.95	5.12	1.01	0.47	1.02
Magnetite A	64.32	28.03	2.34	6.32	0.34	0.68	—	—	—	0.26
Shaft furnace dust	62.56	—	0.31	8.16	0.58	0.92	—	—	—	—
Magnesite	—	—	1.20	3.50	42.00	—	—	—	—	2.00
Limestone	—	—	45.4	2.91	6.81	—	—	—	—	—
Quicklime	—	—	80.0	5.00	1.10	—	—	—	—	—

Table 2. Industrial analysis of coke breeze and chemical compositions of the ash wt%

Fixed carbon	Volatile	Organic compounds	Ash (14.00wt%)					
			FeO	CaO	SiO_2	MgO	Al_2O_3	Others
84.00	0.50	1.50	0.14	0.48	7.50	0.15	2.72	2.89

Table 3. Particle parameters of iron fines

Materials	Circularity	Maximum particle size / mm	Minimum particle size / mm	Average particle size / mm	Aspect ratio	Median particle size / mm
V–Ti–Cr fines	0.87	0.89	0.002	0.17	1.38	0.210
Magnetite A	0.81	0.69	0.002	0.13	1.39	0.056

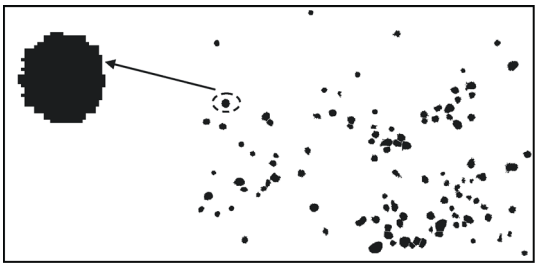

Fig. 1. Morphological appearance of V–Ti–Cr fines.

The XRD pattern of the V–Ti–Cr shown in Fig. 2 indicates that the chemical speciation of the titanium minerals is titanium–magnetite. In the magnetite, V mainly occurs isomorphically, while Cr also occurs isomorphically, forming chromium–magnetite. Iron and titanium in the ore are dense and symbiotic, mainly occurring in the form of magnetite (Fe_3O_4/$Fe_{2.95}O_4Si_{0.05}$) and ilmenite ($FeTiO_3$), while TiO_2 monomer does not exist in V–Ti–Cr fines; these results are in agreement with the relevant mineralogical analysis of V–Ti-magnetite [13–14].

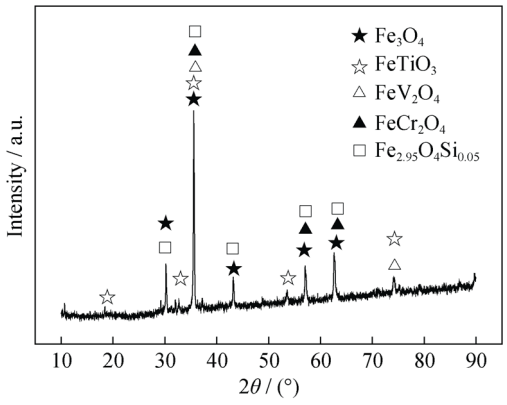

Fig. 2. XRD pattern of V–Ti–Cr fines.

2.2. Experimental methods

The sintering tests were conducted in a pilot-scale pot. The tests covered blending, mixing, granulation, ignition, sintering, cooling, crushing, and treatment of the cooled sinter. The mass fraction of V–Ti–Cr fines was 50wt%; the mass fraction of magnetite A was approximately 9.16wt%, and the mass fraction of shaft furnace dust was 4.5wt%. The mass fraction of return fines was 14.0wt%, and the coke content was 5.0wt%. The basicity (R = CaO/SiO_2) was adjusted to 2.10 by limestone or/and quicklime. The reference ore matching scheme of the V–Ti–Cr sintering pot test is shown in Table 4.

The sinter blend mixture used was a twice-mixed granulation. First, the raw materials were loaded in an iron plate according to Table 4 and blended. They were then wetted for 2–12 min by adding 6.0wt%–9.0wt% moisture, and the mixture was finally loaded into a granulation drum with a diameter of 600 mm and a length of 1400 mm. The granulation of the sinter mixture was performed at 15 r/min for 2–8 min. Some of the granulated sinter mixture was sampled to measure the moisture, size distributions, and permeability. The rest was loaded into a ϕ150 mm × 500 mm sinter pot with a 1-kg hearth of V–Ti–Cr sinter sizing at 10–16 mm. After ignition at 1000°C for 2 min, sintering proceeded until the end point of sintering when the temperature of the flue gas reached the peak value. Subsequently, the sample was cooled for 5 min at 5 kPa suction. The sinter plus was then crushed by a rake crusher with 40-mm gaps between rakes, followed by a shattering test, where crushed sinter was dropped three times from a height of 2 m. Finally, the sinter was screened into five size fractions (>40 mm, 25–40 mm, 10–25 mm, 5–10 mm, and <5 mm) for further evaluation of metallurgical properties. The sintering test parameters are listed in Table 5.

Table 4. Reference ore matching scheme of V–Ti–Cr sintering pot test wt%

Item	V–Ti–Cr fines	Magnetite A	Shaft furnace dust	Magnesite	Limestone	Returns
Reference	50.00	9.16	4.50	2.00	15.34	14.00

Table 5. Parameters of sintering test

Bed height: 500 mm	Sintering pot diameter: 150 mm
Ignition pressure: 5.0 kPa	Exhausting pressure: 10.0 kPa
Ignition temperature :1000°C	Ignition time: 2 min
Carbon content in blend mix: 5.0wt%	Moisture: 6.0wt%–9.0wt%
Return fines content: 14.0wt%	Wetting time: 2–12 min
Basicity (R=CaO/SiO_2): 2.10	Pelletizing time: 2–8 min

3. Results and Discussion

3.1. Effect of quicklime on sintering

Limestone was replaced by 2wt%, 5wt%, and 6.5wt% of quicklime based on a reference ore-matching scheme. The basicity (R = CaO/SiO_2) was adjusted to 2.10 using limestone, the granulation time was fixed to 5 min, the mixture moisture was maintained at 7.0wt%, and the coke ratio was set at 5.0wt%.

The effect of quicklime dosage on the sintering behavior is shown in Fig. 3. As the quicklime dosage increases, the vertical sintering speed increases from 16.39 to 18.86 mm/min, the yield increases from 56.30wt% to 60.3wt%, the TI increases from 55.36wt% to 57.50wt%, and the productivity increases from 0.97 to 1.20 $t{\cdot}m^{-2}{\cdot}h^{-1}$.

The indicators increase at a higher rate before the quicklime dosage reaches 5.0wt%, and no further positive effect is observed once the quicklime dosage exceeds 5.0wt%. Quicklime can slake into hydrated lime $Ca(OH)_2$ when it meets water in the sinter mixing and granulation stages. In addition, the temperature of the sinter mixture is increased by the exothermic reactions of hydration, and granulation is also improved by bonding of $Ca(OH)_2$, which can reduce moisture condensation in the bottom layer of the sinter bed and improve the granule strength [15–16]. This decreases resistance in the sintering process and improves the sintering indicators. Meanwhile, the hydrated lime $Ca(OH)_2$ slaked by quicklime is conducive to the generation of calcium ferrite in the solid phase, improving the sinter strength by increasing the calcium ferrite content.

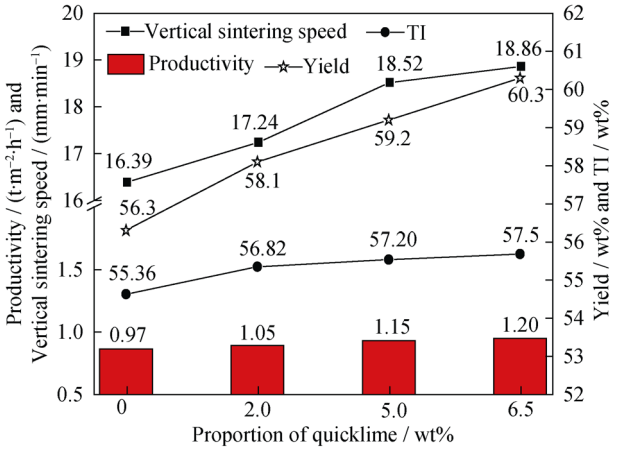

Fig. 3. Effect of quicklime proportion on V–Ti–Cr sintering.

More moisture is needed to consume and carry out the non-complete mineralization of part of the quicklime. Due to the shortage of moisture, some white flakes of free quicklime can be found in the mixture once the quicklime dosage is increased to 5.0wt%. The quality of free quicklime in the mixture is not good enough to improve the overall quality of the sinter. Therefore, the optimum quicklime dosage is 5.0wt%.

3.2. Effect of mixture moisture on sintering

During sintering, the quicklime dosage was 5.0wt%, and the basicity (R = CaO/SiO_2) was adjusted to 2.10 using limestone. The granulation time was 5 min and the mixture moisture contents were 6.0wt%, 7.0wt%, 7.5wt%, 8.0wt%, and 9.0wt%. The effect of mixture moisture on the sintering behaviors is shown in Fig. 4.

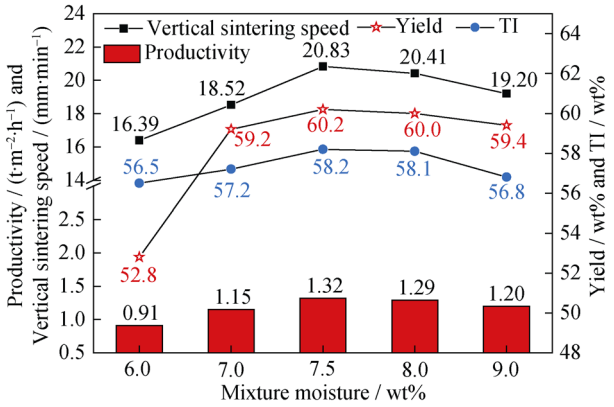

Fig. 4. Effect of mixture moisture on V–Ti–Cr sintering.

As more quicklime is incorporated into the sinter mixture, more moisture must be added to guarantee full quicklime hydration, more heat is released, and more bonding of hydrated lime occurs, improving the granulation and sintering. The vertical sintering speed, yield, TI, and productivity first increase, reaching maximum values of 20.83 mm/min, 60.20wt%, 58.20wt%, and 1.32 $t{\cdot}m^{-2}{\cdot}h^{-1}$, respectively, at a mixture moisture content of 7.5wt%. Once the moisture of the sinter mixture exceeded 8.0wt%, the vertical sintering speed, yield, TI, and productivity dropped slightly; these parameters dropped dramatically when the moisture content exceeded 9.0wt%. The heat provided to generate the liquid phase is insufficient for sustaining evaporation once the moisture exceeds 7.5wt% with a fixed amount of fuel. Additionally, the excess moisture fills the pores of the balls, causing them deform and coalesce. This results in the small particles becoming too large to easily produce enough of the liquid phase. Furthermore, the thickness of the sintered wet layer increases with excess moisture, while the material layer permeability decreases. Therefore, the vertical sintering speed, yield, TI, and productivity drop. Thus, the results suggest that the highly sensitive moisture fluctuations in the active zone of the V–Ti–Cr mixture should be strictly controlled.

3.3. Effect of wetting time on sintering

For this portion of the study, the quicklime dosage was 5.0wt%, the basicity (R = CaO/SiO_2) was adjusted to 2.10 using limestone, the granulation time was 5 min, and the mixture moisture was maintained at 7.5wt%. The effect of wetting time on the sintering behaviors is shown in Fig. 5.

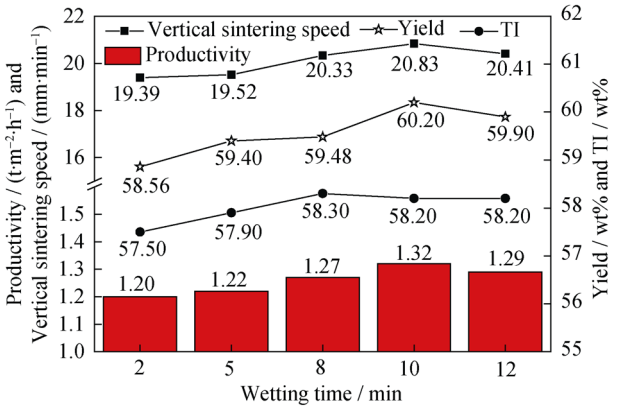

Fig. 5. Effect of wetting time on V–Ti–Cr sintering.

Fig. 5 shows that the indicators trend upward with increases in wetting time; the vertical sintering speed and productivity reach maximum values of 20.83 mm/min and 1.32 $t{\cdot}m^{-2}{\cdot}h^{-1}$, respectively, when the wetting time is 10 min. Once the wetting time exceeds 10 min, the vertical sintering speed and productivity decrease because the temperature increase of the sinter mixture due to exothermic reactions of hydration is reduced. In conclusion, the optimum wetting time is 10 min.

3.4. Effect of granulation time on sintering

For this part of the study, the quicklime dosage was 5.0wt%, the basicity (R = CaO/SiO_2) was adjusted to 2.10 using limestone, the wetting time was 10 min, and the mixture moisture was maintained at 7.5wt%. The effect of granulation time on the sintering behavior is shown in Fig. 6.

Fig. 6 reports the effect of granulation time on V–Ti–Cr sintering, clearly indicating that the indicators increase as the granulation time increases. The vertical sintering speed, yield, TI, and productivity reach maximum values of 21.28 mm/min, 60.50wt%, 58.26wt%, and 1.36 $t{\cdot}m^{-2}{\cdot}h^{-1}$, respectively, when the granulation time is 8 min. With increases in

granulation time, the quasi-particle index GI_0, the average diameter of the ball d, the pelletizing efficiency E, and the anti-chalking index B of the V–Ti–Cr fines also increase. The increases in GI_0, d, E, and B then lead to increases in material layer permeability, improving the indicators, especially when the granulation time is between 2 and 4 min. When the granulation time exceeds 5 min, the ball volume of the V–Ti–Cr fines grows rapidly, and some of the balls are damaged by subsequent impact forces during the granulation process, resulting in the effects of granulation time being less evident. On the basis of the above results, we suggest that the granulation time should be controlled between approximately 5 and 8 min.

3.5. Effect of granulation on sintering material layer permeability

The granulation indices of the reference mixture and mixture II (the mixture with 5.0wt% quicklime, 7.5wt% moisture, a wetting time of 10 min, and a granulation time of 8 min) were investigated. The results are shown in Table 6 and Fig. 7.

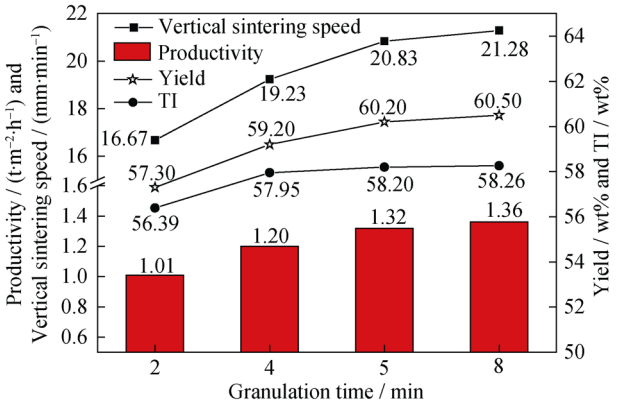

Fig. 6. Effect of granulation time on V–Ti–Cr sintering.

Table 6. Size distribution of V–Ti–Cr balls wt%

Item	+8 mm	8–5 mm	5–3 mm	3–2 mm	2–1 mm	1–0.25 mm	–0.25 mm	d / mm
Reference	3.75	6.86	9.38	12.65	24.28	20.67	22.41	2.05
II	5.56	7.65	12.86	20.80	18.28	16.26	18.59	2.56

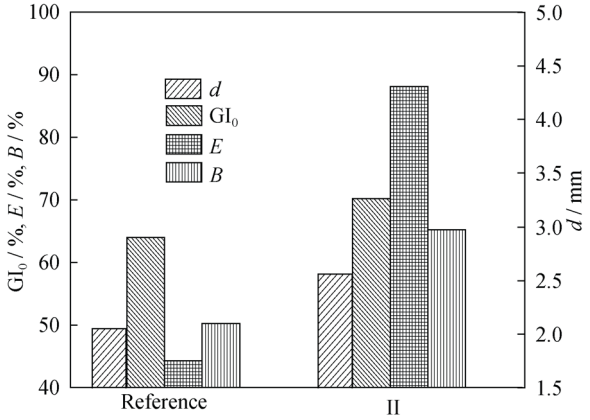

Fig. 7. Effect of enhanced granulation on granulation index of V–Ti–Cr mixture.

The parameters d, GI_0, E and B are defined and calculated as follows.

(1) Average particle size d:

$$d = \frac{\sum w_i d_i}{\sum w_i},$$

where w_i is the mass fraction of grain i, and d_i (mm) is the average particle size of grain i.

(2) quasi-particle index GI:

$$GI = \left(\frac{A_1 - B_1}{A_1} + \frac{A_2 - B_2}{A_2}\right) \times 100\%,$$

where A_1 is the mass fraction of the 0.5–0.25 mm size fraction before granulation, B_1 is the mass fraction of the 0.5–0.25 mm size fraction after granulation, A_2 is the mass fraction of the <0.25 mm size fraction before granulation, and B_2 is the mass fraction of the <0.25 mm size fraction after granulation.

Generally, the second term in the right-hand side of the above formula was used for the calculation:

$$GI_0 = \left(\frac{A_2 - B_2}{A_2}\right) \times 100\%,$$

(3) pelletizing efficiency E:

$$E = \frac{q_2 - q_1}{q_1} \times 100\%,$$

where q_1 is the mass fraction of >3 mm size fraction materials before granulation, and q_2 is the mass fraction of >3 mm size fraction materials after granulation.

(4) Anti-chalking Index B:

$$B = \left(1 - \frac{W_2 - W_1}{W_0 - W_1}\right) \times 100\%,$$

where W_0 is the mass fraction of <0.25 mm size fraction materials before granulation, W_1 is the mass fraction of <0.25 mm size fraction materials after granulation, and W_2 is the mass fraction of <0.25 mm size fraction of granulation materials after strength testing.

(5) permeability p (Carman equation):

$$p = \frac{0.2g\varepsilon^{\alpha}}{\eta S^2} \quad (Re \leq 2300),$$

$$p = \frac{1.629g^{0.526}\varepsilon^{1.58}}{\eta^{0.053}S^{0.579}\rho^{0.474}} \quad (Re > 2300)$$

according to the Voice equation

$$p = \frac{F}{A} \cdot \frac{h^m}{s^n},$$

where p is the permeability, g is the acceleration due to gravity, ε is the porosity, η is the gas viscosity, S is the specific surface area of material pellets, ρ is the gas density, F is the airflow, A is the ventilation area, h is the material layer height, s is the negative pressure, and m and n is coefficients, where $m = n = 0.6$.

As can be observed in Table 6 and Fig. 7, compared to the reference mixture, the average particle size of d in mixture II increases from 2.05 to 2.56 mm, which is appropriate within the scope of 2.4–2.6 mm [17]. However, the 2–5 mm size fraction of mixture II is only 33.66wt%, much less than the 50wt% content of the 2–5 mm fraction in ordinary iron ore. The proportion of the <0.25 mm size fraction decreases from 22.41wt% to 18.59wt%, GI_0 improves from 64.03% to 70.16%, E increases from 44.27% to 88.09%, and B increases from 50.26% to 65.23%, all of which improve the porosity ε of the material layer. According to the Kozeny–Carman equation, the material layer permeability p is related to both the material layer traits (ε, S) and gas properties (η, ρ). In addition, S, η, and ρ are all stationary, and the material layer traits and gas properties are under the same conditions; thus, p will increase with improvements in ε. From the Voice equation, we know that F is proportional to p when h, s, and A are all stationary. Because F increases with the improvement of p, the vertical sintering speed increases, and the increase of the material layer's oxidizing atmosphere is conducive to the generation of calcium ferrite [18–20], improving both the mineral composition of the sinter and the sintering behavior.

3.6. Consolidation mechanism of V–Ti–Cr fines

The petrology of mineral V–Ti–Cr sinters (reference and II) has been analyzed. The mineral composition of the V–Ti–Cr sinter is shown in Table 7.

Table 7. Mineral composition of V–Ti–Cr sinters vol%

Item	Magnetite	Hematite	Perovskite	Silicate	Calcium ferrite	Glass
Reference	36–38	16–18	12–15	14–16	8–10	7–9
II	30–32	18–20	10–12	15–18	12–14	5–8

The results show that the mineral composition of V–Ti–Cr sinter is complex, and that the mineral composition is primarily magnetite (mostly containing Ti, V, Cr, Mg, etc.), hematite (mostly containing Ti, V, Cr, Mg, etc.), silicate (dicalcium silicate, iron olivine, etc.), calcium ferrite, glass, and perovskite.

The consolidation of a V–Ti–Cr sinter requires an approximately 14vol% calcium ferrite liquid-state consolidation (Figs. 8(b) and (d)) and an approximately 15vol% silicate liquid-state (Figs. 8(a) and (c)) supplemented by a solid-state reaction and the recrystallization of Fe_3O_4 (Figs. 8(c) and 9). The amount of liquid phase, especially calcium ferrite, required to harden a V–Ti–Cr sinter is much lower than that required for ordinary iron ore sinters, which require 30vol%–40vol% calcium ferrite. Furthermore, some perovskite, a noteworthy mineral that should be taken in account with V–Ti sinters, is needed perovskite weakens the role of the bonding phase and makes the sinter susceptible to cracking when struck by an external force when perovskite disperses in the slag phase and in the iron minerals. Compared to ordinary sinters, the calcium ferrite content in a V–Ti–Cr sinter is relatively low, and the perovskite occupies more volume, leading to poor TI and RDI in V–Ti sinters [21].

In addition, solid-state recrystallization plays an important role in the consolidation of a V–Ti–Cr sinter, as shown in Figs. 8 and 9. EDS patterns of a V–Ti–Cr sinter in different micro-zones under SEM are shown in Fig. 10. The solid-state reaction temperature (T_r) is equal to approximately 0.57 T_m (the melting temperature) in the sintering process; when the temperature is higher than the T_r, particles inside the crystal lattice of magnetite obtain enough energy to overcome bond barriers and diffuse onto the surface. This forms connecting bridges between the ore particles (indicated by the arrowheads in Figs. 8(c) and 9), resulting in the recrystallization and crystal growth of magnetite. This recrystallization of magnetite is one of the solidification patterns of a V–Ti–Cr sinter. In addition, the peak sintering temperature reaches 1450–1500°C and surpasses the melting points of fayalite (1205°C) and Ca–Fe olivines (1150°C; Fig. 8(d)).

Overall, the crystallization of a V–Ti–Cr sinter is complex; magnetite is mostly distributed jointly among calcium ferrite, perovskite, and silicate (Fig. 8). Hematite is mainly concentrated at the mineral edge (Fig. 8(a)), and bonding phase content is minimal, especially for calcium ferrite with good strength. Solid-state recrystallization plays an important role in the consolidation of a V–Ti–Cr sinter (Figs. 8 and 9).

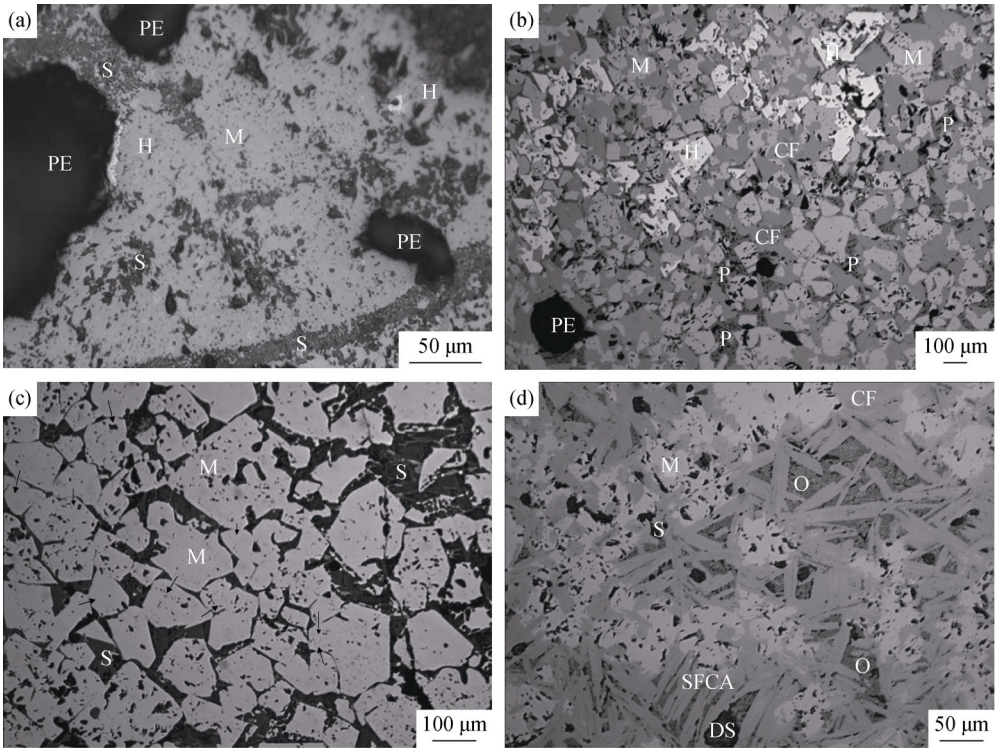

Fig. 8. Mineral structures of V–Ti–Cr sinter (II) (M: magnetite; H: hematite; S: silicate; CF & SFCA: calcium ferrite; P: perovskite; PE: pore; O: olivine; DS: dicalcium silicate).

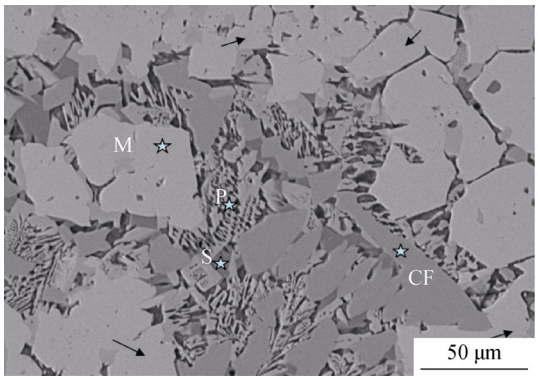

Fig. 9. SEM image of V–Ti–Cr sinter (II) (M: magnetite; S: silicate; CF: calcium ferrite; P: perovskite).

When the ratio of V–Ti–Cr fines reaches 50wt% in the mixture, priority will be given to the production of perovskite rather than calcium ferrite during sintering. Perovskite does not have bonding effects and disperses in the slag phase and the iron minerals, which weakens the role of the silicate bonding phase along with the crystal stock between hematite and magnetite (Fig. 8(b)). In order to obtain a high quality V–Ti–Cr magnetite sinter, the content of the liquid-phase should increase to approximately 40%, and the content of SiO_2 should be controlled at approximately 5.0wt%. The amount of calcium ferrite should be increased, and the amount of perovskite should be decreased by increasing the ratio of added ordinary ores to a maximum of 47wt% [22]. Moreover, the temperature and coke content should be considered carefully due to their influences on solid-state recrystallization. When there is a variation in the ratio of V–Ti–Cr fines, the optimal coke content must be adjusted for the high melting point of V–Ti–Cr fines. The optimal coke content of a sinter with 13wt% V–Ti–Cr fines is 4.0wt%–4.5wt% [23]. Further studies are underway to determine how to achieve the best possible V–Ti–Cr magnetite sinter.

4. Conclusions

Sinter pot tests on V–Ti–Cr fines were carried out, and the effects of quicklime dosage, mixture moisture, wetting time, and granulation time on the sintering behaviors of V–Ti–Cr fines were investigated. Furthermore, to gain a better understanding of the effects of granulation, material layer permeability was analyzed, and the granulation index of a reference mixture and the mixture II were studied. In addition, mineral petrology and SEM-EDS techniques were used to characterize the V–Ti–Cr sinter and thus reveal the consolidation mechanism. The following conclusions can be drawn from this work.

(1) V–Ti–Cr fines have poor granulation efficiency, and

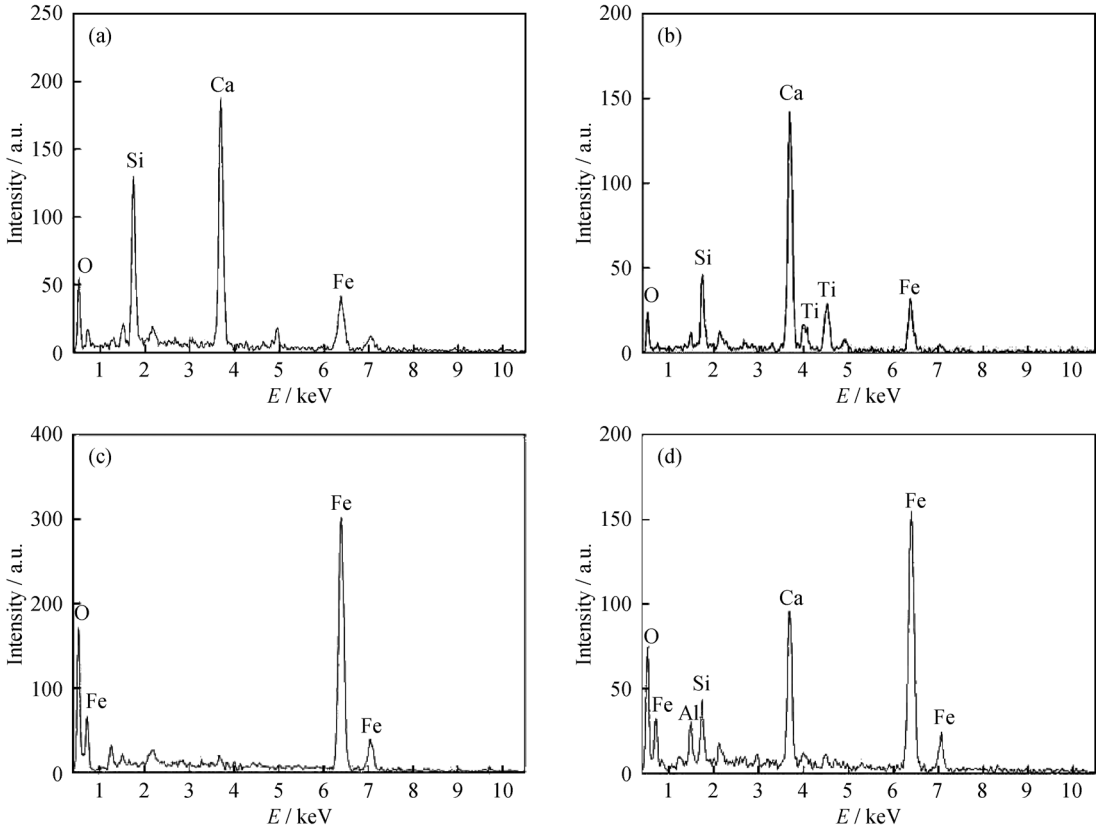

Fig. 10. EDS patterns of micro-zone S (a), micro-zone P (b), micro-zone M (c), and micro-zone CF (d).

quicklime dosage, mixture moisture, wetting time and granulation time all have important effects on the sintering behaviors. The optimum conditions are as follows: quicklime dosage, 5wt%; mixture moisture, 7.5wt%; wetting time, 10 min; granulation time, 5–8 min. The vertical sintering speed, yield, TI, and productivity are 21.28 mm/min, 60.50wt%, 58.26wt%, and 1.36 $t \cdot m^{-2} \cdot h^{-1}$, respectively. Additionally, d, GI_0, E, and B increase from 2.05 mm, 64.03%, 44.27%, and 50.26% to 2.56 mm, 70.16%, 88.09%, and 65.23%, respectively.

(2) The consolidation of a V–Ti–Cr sinter requires an approximately 14vol% calcium ferrite liquid-state consolidation and an approximately 15vol% silicate liquid-state supplemented by a solid-state reaction and recrystallization of magnetite. Compared to an ordinary sinter, the calcium ferrite content in a V–Ti–Cr sinter is relatively low, and the perovskite content is high, resulting in poor sinter results.

(3) In order to obtain a high quality V–Ti–Cr sinter, the amount of calcium ferrite should be increased, while the content of perovskite should be decreased. The effects of solid-state recrystallization should also be considered. Further studies are needed to determine how to achieve the best possible V–Ti–Cr sinter.

Acknowledgements

The authors are grateful to the National High Technology Research and Development Program of China (Nos. 2012AA062302 and 2012AA062304), the Program of the National Natural Science Foundation of China (Nos. 51090384 and 51174051), and The International Cooperation of the Ministry of Science and Technology of China (No. 2012DFR60210) for support of this research. We would also like to thank Professor Xing-min Guo, University of Science and Technology Beijing, for his help in the petrology of mineral experiments.

References

[1] R.R. Moskalyk and A.M. Alfantazi, Processing of vanadium: a review, *Miner. Eng.*, 16(2003), No. 9, p. 793.

[2] K.J. Hu, G. Xi, and J. Yao, Status quo of manufacturing techniques of titanium slag in the world, *World Nonferrous Met.*, (2006), No. 12, p. 26.

[3] X. Xue, Research on direct reduction of vanadictianomagnetite, *Iron Steel Vandium Titanium*, 28(2007), No. 3, p. 37.

[4] J. Deng, X. Xue, and G.G. Liu, Current situation and development of comprehensive utilization of vanadium-bearing titanomagnetite at Pangang, *J. Mater. Metall.*, 6(2007), No. 2,

p. 83.

[5] H.V. Vidyashankar and S. Govindaiah, Ore petrology of the V–Ti magnetite (lodestone) layers of the Kurihundi area of Sargur schist belt, Dharwar craton, *J. Geol. Soc. India*, 74(2009), No. 1, p. 58.

[6] D. Beura, D. Acharya, P. Singh, and S. Acharya, Högbomite associated with vanadium bearing titaniferous magnetite of Mafic-Ultramafic suite of Moulabhanj igneous complex, Orissa, India, *J. Miner. Mater. Charact. Eng.*, 8(2009), No. 9, p. 745.

[7] X.G. Si, X.G. Lu, C.W. Li, C.H. Li, and W.Z. Ding, Phase transformation and reduction kinetics during the hydrogen reduction of ilmenite concentrate, *Int. J. Miner. Metall. Mater.*, 19(2012), No. 5, p. 384.

[8] S.Y. Chen and M.S. Chu, Metalizing reduction and magnetic separation of vanadium titano-magnetite based on hot briquetting, *Int. J. Miner. Metall. Mater.*, 21(2014), No. 3, p. 225.

[9] M. Zhou, S.T. Yang, T. Jiang, and X.X. Xue, Influence of basicity on high chromium vanadium– titanium magnetite sinter properties, productivity and mineralogy, *JOM*, 67(2015), No. 5, p. 1203.

[10] B.C. Jena, W. Dresler, and I.G. Reilly, Extraction of titanium, vanadium, and iron from titanomagnetite deposits at Pipestone Lake, Manitoba, Canada, *Miner. Eng.*, 8(1995), No. 1-2, p. 159.

[11] K.C. Sole, Recovery of titanium from the leach liquors of titaniferous magnetites by solvent extraction: Part 1. Review of the literature and aqueous thermodynamics, *Hydrometallurgy*, 51(1999), No. 2, p. 239.

[12] H.G. Du, *Principle of Blast Furnaces Melting Vanadium–Titanium Magnetite*, Science Press, Beijing, 1996, p. 9.

[13] Y. Zhang, M. Zhou, M.S. Chu , X.X. Xue, and M.F. Jiang, Basic sintering characteristics of imported vanadium and titanium magnetite with high Chrome content, *Iron Steel*, 47(2012), No. 12, p. 18.

[14] Y. Zhang, M. Zhou, M.S. Chu, and X.X. Xue, Sintering experiments of high-Cr vanadium and titanium magnetite, *J. Northeast. Univ. Nat. Sci.*, 34(2013), No. 3, p. 383.

[15] D.Q. Zhu, K.C. Zhang, J. Pan, X.H. Fan, Y.M. Hu, and C. John, Effect of fluxes on high iron and low silica sintering, *J. Cent. South Univ. Technol.*, 10(2003), No. 3, p. 177.

[16] Y. Sassa, H. Ishii, and M. Nakajima, Effect of amount of CaO added on burnt quasi-particles strength, *Nisshin Steel Tech. Rep.*, 67(1993), p. 1

[17] S.D. Li, Research on granulation of mix iron fines, *Sintering Pelletizing*, 13(1988), No. 6, p. 7.

[18] S.J. Zhang and S.T. Wang, Formation mechanism of acicular calcium ferrite, *Iron Steel*, 27(1992), No. 7, p. 7.

[19] X.J. Huang, Y.F. Guo, J. Zhang, and X.M. Guo, Effect of oxygen partial pressure on the sintering process of iron ores, *J. Univ. Sci. Technol. Beijing*, 35(2013), No. 12, p. 1565.

[20] D.Q. Zhu, K.C. Zhang, A.P. He, X.H. Fan, X.Z. Zeng, and L.H. Xiao, The effect of enhances granulating on high Fe and low SiO_2 sinter, *Sintering Pelletizing*, 28(2003), No. 1, p. 9.

[21] Y.Q. Bai, S.S. Cheng, and Y.M. Bai, Analysis of vanadium-bearing titanomagnetite sintering process by dissection of sintering bed, *J. Iron Steel Res. Int.*, 18(2011), No. 6, p. 8.

[22] M. Zhou, S.T. Yang, T. Jiang, and X.X. Xue, Influence of MgO in form of magnesite on properties and mineralogy of high chromium, vanadium, titanium magnetite sinters, *Ironmaking Steelmaking,* 42(2015), No. 3, p. 217.

[23] M. Zhou, *Fundamental Investigation on Cr-bearing Vanadium and Titanium Magnetite Ore in Sintering and Iron-making Process* [Dissertation], Northeastern University, Shenyang, 2015, p.111.